RESEARCH ARTICLE

Restructuring and Activation of Cu(111) under Electrocatalytic Reduction Conditions

Dongfang Cheng, [a] Ziyang Wei, [b] Zisheng Zhang, [b] Peter Broekmann, [c] Anastassia N. Alexandrova*, [b] [d] and Philippe Sautet* [a], [b], [d]

[a] D. Cheng, Prof. P. Sautet
Department of Chemical and Biomolecular Engineering, University of California, Los Angeles, CA, 90095, USA.
E-mail: ana@chem.ucla.edu, sautet@ucla.edu
[b] Z. Wei, Z. Zhang, Prof. A. Alexandrova, Prof. P. Sautet
Department of Chemistry and Biochemistry, University of California, Los Angeles, CA, 90095, USA.
[c] Prof. P. Broekmann
Department of Chemistry and Biochemistry, University of Bern, Freiestrasse 3, Bern 3012, Switzerland.
[d] Prof. A. Alexandrova, Prof. P. Sautet
California NanoSystems Institute, Los Angeles, CA, 90095, USA.

Abstract: The dynamic restructuring of Cu surfaces in electroreduction conditions is of fundamental interest in electrocatalysis. We decode the structural dynamics of a Cu(111) electrode under reduction conditions by joint first-principles calculations and operando electrochemical scanning tunneling microscopy (ECSTM) experiments. Combining global optimization and grand canonical density functional theory, we unravel the potential- and pH-dependent restructuring of Cu(111) in acidic electrolyte. At reductive potential, Cu(111) is covered by a high density of H atoms and, below a threshold potential, Cu adatoms are formed on the surface in a (4×4) superstructure, a restructuring unfavorable in vacuum. The strong H adsorption is the driving force for the restructuring, itself induced by electrode potential. On the restructured surface, barriers for hydrogen evolution reaction steps are low. Restructuring in electroreduction conditions creates highly active Cu adatom sites not present on Cu(111).

Introduction

Electrocatalysis is one of the pillars of a future sustainable energy landscape, enabling chemical storage of renewable energy and allowing the production of valuable molecules[1]. Hydrogen interaction with metal electrodes is of fundamental importance in electrocatalysis, where hydrogen evolution reaction (HER) plays a central role[2]. HER is both a highly desired reaction to transform electrical energy into chemical energy in the form of molecular hydrogen in water electrolysis and an unwanted side reaction for many other electrochemical processes, for example, metal electroplating[3], electrosynthesis[4] and electrochemical CO_2 reduction reaction (CO_2RR)[1b, 5]. For the case of CO_2RR, to date, Cu is proven to be the only transition metal that can catalyze CO_2 to valuable multi-carbon products like ethylene and ethanol[6]. Experimental evidence suggests that on the one hand, the structure of the Cu catalyst is of key importance in controlling the selectivity between H_2 and hydrocarbon species as products[7], meanwhile, the Cu surface undergoes dramatic restructuring during the electrochemical reduction reaction[7-8]. However, these restructuring events, and their impact on the catalytic performance, are far from being understood today.

One intriguing example is the Cu(111) surface in acidic conditions. During a negative potential sweep, a change of structure of the surface has been observed by operando STM at the onset of HER. A superstructure is seen, associated with a (4×4) unit cell with respect to the Cu(111) 1×1 lattice[9]. In addition, a unique redox wave at -0.35 V vs RHE has been found on Cu(111) surfaces in voltammetry cycles, while no such distinct signatures were found on Cu (100) and Cu (110) surfaces[10]. Several hypotheses have been proposed to explain these phenomena, such as H intercalation in the Cu surface to form a hydride compound or H-mediated restructuring[10]. Unfortunately, no atomic structural model of this restructuring of Cu(111) in electroreduction conditions has been established yet. Very recent work by Sargent et al[11] showed a remarkable performance of Cu catalyst in strong acid electrolytes toward CO_2 conversion to multi-carbon products, indicating the feasibility and prospects of acidic CO_2RR in the future. However, the lack of knowledge of surface restructuring impedes the rational design of improved catalytic active sites for acidic CO_2RR[12]. Modeling studies for HER in the literature are performed on conventional non-reconstructed surface models such as the Cu(111) surface or stepped surfaces[13], but this approach is not sufficient to describe the realistic surface state under operational conditions. As a result, the impact of surface restructuring on HER electrocatalytic activity, promoting or decreasing it, is unknown. Furthermore, the electrochemical interface is often approximated by a neutral, non-charged interface. However, the dynamic behavior of the adsorbates on the electrocatalyst strongly depends on the electrode potential and solution pH, which cannot be practically handled by such methods.

Here, we explore the potential-dependent restructuring of the Cu(111) surface induced by H adsorption under electrochemical reduction in acidic conditions by a combination of first-principles simulations and operando electrochemical scanning tunneling microscopy (ECSTM) experiments. Although the general motivation for choosing Cu(111) is CO_2RR, we will restrict ourselves here to mildly negative potentials, before the onset for hydrocarbon product formation, since in situ STM data can be obtained for these experimental conditions. The surface configurations are efficiently sampled by a grand canonical genetic algorithm (GCGA) global optimization method, and grand canonical density functional theory calculations (GCDFT) permitting the explicit potential modelling by surface charging in an implicit electrolyte. Specific surface structures were found stable at reducing potential, corresponding to a (4×4) supercell reconstruction bearing one additional Cu adatom, decorated and stabilized by high coverage of H adsorbates. The simulated STM images match the potential-dependent experimental operando STM images, enabling a detailed interpretation of the underlying surface structures and validating that the theoretically proposed restructured surfaces are the ones occurring on Cu(111). Jointly,

these approaches reveal, upon shifting the potential to a more negative value, the formation first of a (4×4) H adlayer, followed by Cu restructuring by adatom formation below a threshold potential (seen experimentally at -0.32 V vs SHE when pH = 2). Higher pH conditions are explored computationally and are shown to decrease the H coverage and to impede the reconstruction. Furthermore, the stronger adsorption of H on the restructured Cu surface is shown to be the driving force for the Cu adatom formation. Mechanistic studies using a hybrid solvent model show that HER steps are fast on the restructured Cu surface, making the Cu adatoms highly active for HER, and implying that the surface structure is involved in fast kinetic transformations between the various intermediates of the reaction. Operando STM provides a time-average imaging of this dynamic reactive surface.

Results and Discussion

Determining the configurations of the Cu-H surface at given electrochemical conditions is a significant challenge since the hydrogen coverage on the Cu surface varies with the pH and electrode potential, and the surface possesses a large number of degrees of freedom for possible restructuring. Here, we explored the surface ensemble of configurations for Cu(111) in electrocatalytic conditions with various hydrogen coverage using GCGA[14], an efficient global optimization method aimed at exploring structures at a fixed chemical potential rather than a fixed composition. Since the pristine Cu(111) surface may be hard to restructure, we seeded the search with several initial Cu configurations with varying densities of Cu adatoms and Cu vacancies (for details, see methods and Supplementary Figure 1-8).

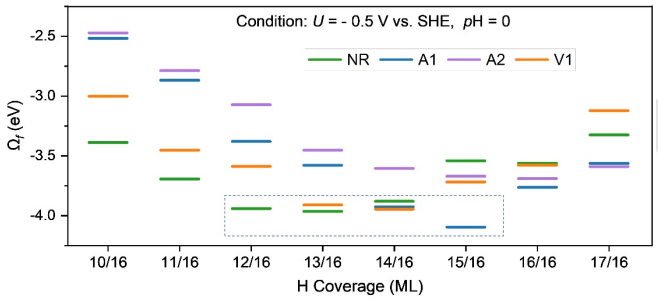

Figure 1. Thermodynamic driving force for Cu(111) restructuring under electro-reduction conditions: Grand Canonical formation free energy (Ω_f) as a function of H coverage at pH = 0 under a potential of -0.5 V vs SHE. Each energy level corresponds to the global minima(GM) at each coverage for the considered surface structure classes, all using a (4×4) supercell of Cu(111): NR: non-reconstructed; A1: with one Cu adatom; A2: with a Cu adatom-dimer; V1: with one Cu vacancy in the surface layer. The dotted box frames the grand-canonical (i.e., variable H coverage) low energy structures, including the most stable (4×4) Cu surface with one adatom (A1) and a 15/16 ML H coverage.

The GCGA method we employed here uses a hydrogen reservoir, and is designed to minimize the coverage-dependent formation free energy (Ω_f):

$$\Omega_f = U - TS - \sum \mu x = E(\text{slab\_}x\text{H}) - E(p\text{Cu}) \pm n\mu(\text{Cu}) - x\mu(\text{H})$$

where the $E(\text{slab\_}x\text{H})$ is the electronic energy of the optimized H-covered structure, $E(p\text{Cu})$ is the energy of pristine non-reconstructed Cu(111), n is the number of adatoms or vacancies, denoted as '-' and '+', respectively. $\mu(\text{Cu})$ is the Cu chemical potential derived from Cu bulk. x is the number of hydrogen and $\mu(\text{H})$ is the H chemical potential, which is dependent on pH and electrode potential, *U*. For simplicity, a series of GCGA has been performed on the different substrates using model conditions of -0.5 V vs SHE and pH of 0, keeping the (4×4) unit cell captured by STM imaging. More detailed potential and pH dependence will be described later. In total, ~10,000 structures were sampled in a broad stoichiometric distribution for Cu_nH_x system. After GCGA sampling, we performed accurate calculations on the global minima (GM) and multiple metastable structures (MS) using grand canonical DFT (GCDFT) calculations[15], i.e. explicitly including the charge polarization resulting from the applied potential, combined with an implicit model of the water solvent and the electrolyte (see methods).

The obtained formation free energies (Ω_f) are shown in Figure 1. For clarity and simplicity, we only include in Figure 1 the most stable configuration found for each important class of initial Cu configurations (NR = non-reconstructed, A1, A2: surface with 1 or 2 adatoms, V1: surface with 1 Cu vacancy in the surface plane) and each considered H coverage, while all MSs for each class are included in Supplementary Information. Configurations with 3 adatoms or with 2 to 4 vacancies were found noncompetitive and are not included in Figure 1 (see Supplementary Figure 7 and 8). Ω_f plots show a convex hull as a function of H coverage for each class of structure, although the different structure models correspond to different optimum H coverage for the considered conditions. While the pristine surface shows an optimal coverage of 13/16ML at -0.5 V vs SHE, surfaces with vacancies or adatoms prefer larger amounts of H, 14/16, 15/16, and 16/16 ML, for V1, A1, and A2 structure classes, respectively. At low H coverage, Cu(111) restructuring is not energetically favorable, but when coverage reaches 14/16 ML a crossover appears and restructuring by adatom or vacancy formation becomes preferred. The restructured surface with the formation of one Cu adatom and an H coverage of 15/16 ML in the (4×4) unit cell is globally the most favored configuration at the selected potential of -0.5 V. This is remarkable since, as we will discuss later, formation of such defects on Cu(111) in vacuum is significantly endothermic.

Before examining these surface structures, we will first determine how their stability depends on electro-reduction conditions, evaluate accurately their potential dependence, and make the link with experimental characterization by operando STM. This will allow us to understand how the Cu(111) surface dynamically responds to the electrode potential and the solution pH, and how the surface configurations under different H coverages can be accessed. The free energy of each most stable surface structure at different H coverages is calculated in the grand canonical ensemble of electrons and adsorbates at various pH and electrode potentials using the surface charging method, which enables us to obtain the potential-dependent electronic free energy of the surface.

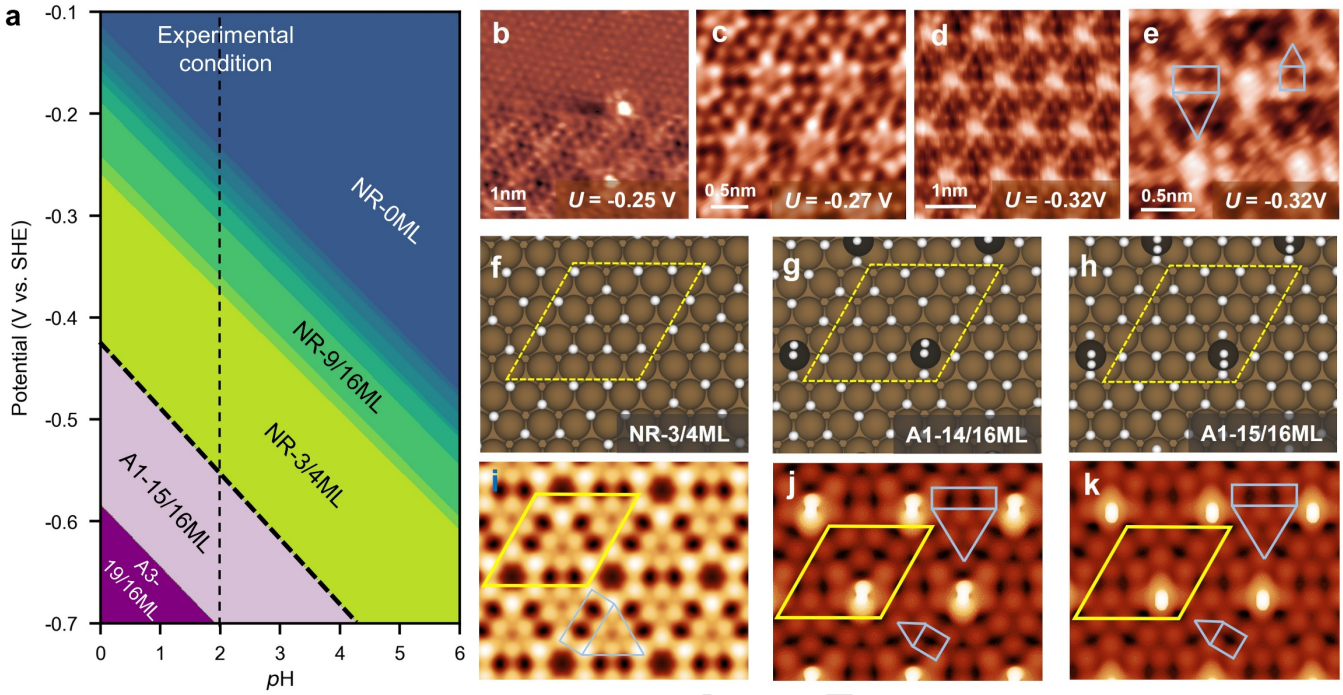

Figure 2. Evolution of the structure of Cu(111) in electroreduction conditions. (a) Surface Pourbaix diagram assuming global thermodynamic equilibrium. The restructured region is shown in pink. Experimental operando STM images of the Cu(111) surface during HER in 5 mM H_2SO_4 solution: (b) working electrode potential U = -0.21 V vs SHE (top part), U = -0.25 V vs SHE (bottom part) (tip bias voltage U_b = 15mV; tunnel current I_t = 10nA); (c) U = -0.27 V vs SHE (U_b = 18mV; I_t = 12nA) (d, e) U = -0.32V vs SHE (U_b = 335mV; I_t = 10nA). Images c, d and e have been slightly rotated to align the dense Cu row with that of the calculations. Top view of simulated atomic structures of (f) NR-3/4ML; (g) A1-14/16ML; (h) A1-15/16ML. Color code: terrace Cu: brown, Cu adatom: black, H: white. Simulated STM images for (i) NR-3/4ML, (j) A1-14/16ML, (k) A1-15/16ML, the bias voltages (U_{bias}) in the STM simulations are all 0.05 V.

In acidic conditions, the first H adsorption and surface restructuring occur at weakly negative potential (Figure 2a). Let us start again at model pH = 0 condition and describe the potential dependence: the proton begins to adsorb on pristine Cu(111) at -0.12 V vs SHE. As the potential becomes more negative, H coverage increases until -0.26 V where an organized H adlayer corresponding to 3/4 ML coverage is formed, combining quasi-square and triangular H adsorption patterns, and remains stable within a large potential range. When the electrode potential reaches -0.42 V vs SHE, the Cu surface is found to restructure to form one Cu adatom in each (4×4) unit cell (structure A1-15). This structure remains stable from -0.42 V to -0.58 V vs SHE, which is a potential window for HER on the Cu(111) surface in an acidic solution. At a more negative potential, calculations predict further restructuring toward adatom trimers and a coverage of H larger than 1 (19/16 ML).

If the pH is increased, the H chemical potential is decreased, so the H^+ reduction to provide adsorbed H atoms becomes more difficult and the H coverage decreases at a fixed potential. All domains in Figure 2a shift to more negative potentials to restore the H coverage required for their formation. Therefore, the reconstruction leading to Cu adatom formation will require more negative potential to occur at higher pH (by ~-0.065 V by pH unit).

Let us now specifically consider pH=2, for which the operando STM experiments were performed. One sees a hexagonal arrangement corresponding to the symmetry of the Cu(111) surface structure at a potential of -0.21 V vs SHE (Figure 2b, top part). This does not mean that the surface is free of adsorbates, and it can be covered with highly mobile H not visible with the STM, the high mobility being expected at low to medium H coverage as shown by calculations. At U = -0.25 - -0.27 V, a first organized (4×4) superstructure is found, combining triangular and square arrangements with a hexagonal arrangement of bright bumps at the apexes (Figure 2b, bottom part, and 2c). A second superstructure is seen at U = -0.32 V, the main difference being the presence of a large bright bump in the center of the hexagon (Figure 2d and e). The direct interpretation of these STM images is not straightforward, but the comparison with the calculated structures and their simulated STM images provides a clear picture. The STM image of the first organized structure that experimentally occurs at the onset potential of -0.26 V (Figure. 2c) corresponds to the simulated image of the calculated NR-3/4ML structure (Figure 2f and i). The Cu surface is not restructured and the STM contrast corresponds to a well-defined configuration of the H atoms in a (4×4) unit cell (Figure 2i). The H atoms are absorbed at hollow sites on the Cu(111) surface and each H atom is associated with a maximum in the image, where the pattern combines triangular and quasi-square motifs, and one quasi-hexagonal motif per unit cell. Hence for that overlayer structure calculations simply assign the contrast in the STM image to the position of H adsorbates. At more negative potential, the Cu surface restructures toward formation of a Cu adatom, giving the A1-15/16 ML structure (Figure 2h). The Cu adatom appears as the main bright feature in the image, while H adatoms provide a

secondary pattern which is similar to that of the NR-3/4ML image (Figure 2k). The Cu adatom is located in the quasi-hexagonal arrangement of H atoms, offering new binding sites for 3 H atoms with respect to the NR-3/4ML structure. One H atom, not directly seen in the STM image, is bridging the adatom and the surface, and an activated molecular H_2 unit is present on the Cu adatom with a H-H distance of 0.804 Å. The observed STM contrast therefore results both from the Cu and H adatoms. The experimental (-0.32 V) and theoretical (-0.55 V at pH = 2) potential where such restructuring of Cu by adatom formation occurs (A1 structure) are slightly different and the small difference (0.23 V) likely results from a combination of approximations in the theoretical modelling (e.g., DFT exchange correlation functional, solvent and electrolyte continuum models). A benchmark study on the potential-induced change of configuration of pyridine on Au (111) using the same approach gave an error in the transition potential of 0.3 V, a value similar to the difference seen here[15c].

The reducing potential for the Cu(111) restructuring by Cu adatom formation is in the HER active region so that the surface of the catalyst is not static but catalyzes the HER (*vide infra*). At even more negative potential, fast hydrogen evolution makes STM imaging very challenging, and the range of potential where further restructuration forming Cu adatom trimers is predicted from calculations could not be experimentally explored.

Next, we can interrogate the driving force producing the reconstruction toward Cu adatoms. Indeed, the formation of Cu adatoms on the bare Cu(111) surface is endothermic by about 0.6 - 0.65 eV in the considered potential range (Figure 3b). The adsorption free energy of H atoms on the Cu surface, resulting from the electroreduction of protons, depends both on the electrochemical potential and on the coverage (Figure 3a). The H adsorption is first stabilized with increasing H coverage reaching an optimum, which depends on the Cu surface structure. When the electrode potential becomes more negative, the H adsorption becomes stronger and the H coverage generally increases. However, for the pristine (111) surface the H coverage reaches a stable 3/4 ML value at -0.26 V with a triangle-square pattern (Figure 2f), and does not increase further until the potential of -0.5 V. Indeed, it is difficult to break this pattern and add other H atoms. Adatom formation creates new sites for H adsorption, since the adatom itself presents a quite low coordination number (3). Hence, the defective surface with the Cu adatom can adsorb more H atoms and provides a more favorable H adsorption free energy at equilibrium. The difference between the optimum adsorption energy for the pristine (NR) surface and the restructured one increases with the potential (Figure 3a). At low potential, this differential H adsorption energy is not large enough to compensate the cost of Cu adatom formation. However, for a potential more negative than a threshold value, the gain in H adsorption energy surpasses the surface rearrangement cost, and the restructuring becomes thermodynamically favored. We therefore conclude that the catalyst restructuring is resulting from an optimization of Cu surface sites to adsorb H and is hence induced by H adsorption, itself induced by the reductive potential.

The relatively weak cohesive energy of Cu compared with other metals is an important factor that affects its restructuring in response to H adsorption[17]. The chemical potential of proton can be modified by solution pH and electrode potential. More negative potential and lower pH will lead to a stronger H adsorption and render the formation of the Cu adatom easier. Thus, regulating

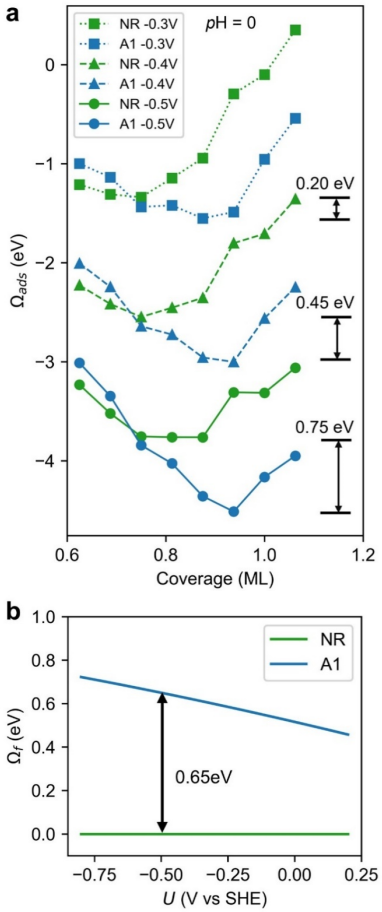

Figure 3. Compared stabilization by H adsorption of non-restructured Cu(111) NR and (4×4) unit cell with a Cu adatom A1. (a) Adsorption free energy as the function of H coverage at different electrochemical potentials and pH = 0. (b) Potential-dependent formation energy of adatom structure in the absence of H adsorption.

solution pH and applied potential can tune the adsorption strength of adsorbates and then induce the defects formation. Further research can extend this design principle to other metals and adsorbates beyond the Cu-H.

Until this point, we have considered proton electrochemical adsorption. However, the considered potential (~ -0.3 - -0.5 V vs SHE) is a typical operational potential for HER in acidic solution[9]. The copper surface will undergo a rapid H exchange with the solution through multiple Volmer-Heyrovsky-Tafel elementary steps to achieve the kinetic reaction steady-state. We now explore the reactive evolution of the restructured Cu surface (starting from the structure A1-15, denoting the GM of the A1 surface that contains 15 adsorbed H atoms, Figure 4a). Using a hybrid solvent model, combining explicit water molecules and implicit dielectric continuum, we evaluate the potential-dependent electrochemical reaction barriers of the various HER elementary steps of the mechanism of Figure 4a, belonging to three classes:

$$* + H^+ + e^- \rightarrow *H \quad \text{(Volmer)}$$

$$*H + H^+ + e^- \rightarrow * + H_2 \quad \text{(Heyrovsky)} \qquad *H + *H \rightarrow H_2 \quad \text{(Tafel)}$$

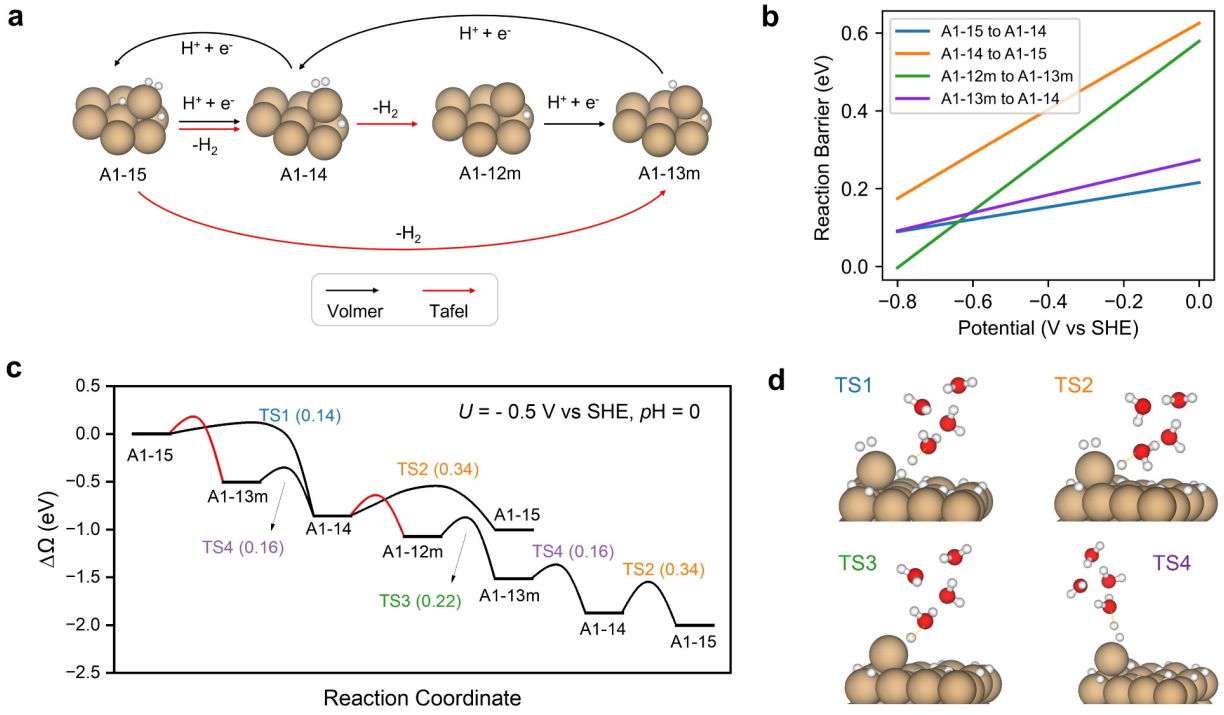

Figure 4. Reactive evolution of the A1-15 structure. (a) Proposed simplified reaction network on A1-15. (b) The reaction barriers for the four proton-coupled electron transfer steps as a function of the potential calculated using the hybrid explict-implicit solvent model. (c) Free energy diagram under -0.5V vs SHE at pH = 0. (d) Transition state (TS) structures for A1-15 to A1-14 (TS1), A1-14 to A1-15 (TS2), A1-12m to A1-13m (TS3) and A1-13m to A1-14 (TS4).

where the * and *H represent the active site and the adsorbed H on the surface, respectively. Since the solution is acidic, solvated H^+ rather than H_2O, is considered as the proton source. For consistency, energies in Figure 4 are calculated without dispersion corrections. Dispersion corrections (see SI) do not change the qualitative results presented here, and energy intervals given in the text below reflect the change in the values when including dispersion corrections (noted without correction/with correction).

Starting from A1-15, the desorption of the H_2 unit is slightly endothermic with a low (uphill) desorption internal energy of 0.23/0.46 eV at -0.5 V vs SHE, but since the H_2 molecule gains entropy upon desorption, the H_2 desorption reaction is exergonic with a (stabilizing) free energy of -0.5/-0.27 eV. This process was found to show no extra barrier on the potential energy surface, besides the positive 0.23/0.46 eV desorption energy, so that the desorption should be fast at room temperature. When the H_2 molecule undergoes the Tafel step and desorbs from the adatom, the H in a *bri*-site between adatom and surface diffuses on top of the adatom (Supplementary Figure 17) and a metastable A1-13 structure is formed (denoted as A1-13m). The single H atom adsorbed on top of the adatom will quickly capture one proton from the solution and an electron from the surface to form an adsorbed H_2 molecule and the A1-14 structure. This Volmer step exhibits only a 0.16/0.17 eV barrier (energy and structure of TS4 on Figure 4b and d). Once the A1-14 structure is formed, it will either accept a proton and go back to A1-15 or undergo a Tafel step, that is the desorption of the H_2 molecule, to form a metastable A1-12 structure (denoted as A1-12m). From the driving force of the negative potential and the activity of the Cu adatom towards protons, A1-12m will rapidly undergo three successive Volmer steps to form the A1-13m and A1-14 intermediates and finally return to A1-15 with proton transfer barriers of 0.22/0.19 eV, 0.16/0.17 eV and 0.34/0.30 eV, respectively (Figure 4 b, d). Finally, A1-15 is likely to form A1-14 via the Heyrovsky step on the *bri*-site H as well. When the proton diffuses from the solution and combines with the *bri*-site H, the adsorbed H_2 molecule on the Cu adatom desorbs and the newly formed H_2 molecule from the reacting proton takes its position. Other pathways that may occur on the A1-15 isomer are discussed in the Supplementary Note 1.

Based on the energy profile (Figure 4c), it can be clearly seen that the reaction barriers for the proton-coupled electron transfer steps on the Cu adatom are low, suggesting that the catalyst dynamically rearranges in electroreduction conditions, hopping between different H coverages, linked by Volmer or Tafel reaction elementary steps, and including the evolution of gas phase H_2. The catalyst surface kinetically evolves along several competing pathways and performs the HER reaction. Low barriers also imply a quick rearrangement, especially for TS1 and TS2, with a fast A1-15/A1-14/A1-15 interchange. Other transformations involving metastable isomers A1-13m and A1-12m are also possible. Altogether, compared to the relatively high barriers (0.5-0.6 eV at -0.5 V vs SHE) of the typical predominant Volmer-Heyrovsky steps on Cu(111) terrace sites from previous work[13c] and from our calculation (Supplementary Figure 24 and 25), the restructured surface with Cu adatoms appears highly active and is proposed to play a key role for the HER activity. Therefore, the reaction conditions created the restructured Cu surface with its highly active site at the Cu

adatom, which can be summarized as the “reaction created the catalyst”.

A key consequence of the dynamic rearrangement of the H adsorbates in electroreduction conditions is that the surface imaged by the STM is not static and that the STM contrast results from averaging between several H configurations (A1-15, A1-14, A1-13m and A1-12m) that rapidly exchange on the surface. Indeed, STM imaging, which necessitates scanning the tip over the image area, is a rather slow technique and the acquisition of one frame requires ~tens of seconds. However, our STM simulations show that all these configurations produce rather similar STM images because the STM contrast is dominated by the presence of the Cu adatom and the organization of H atoms on the terrace (Supplementary Figure 18). As a result, the dynamics created by the HER reactions step for the H atoms near the Cu adatom do not affect the image significantly and a well-defined STM image can be recorded.

Conclusion

Through a combination of theoretical calculations and operando ECSTM experiments, we show that the Cu(111) electrode restructures under electroreduction conditions in acidic electrolyte. Based on global optimization, grand canonical DFT calculations, and STM image simulations compared to the experimental ones, we obtain an atomic scale understanding of the transformation of the Cu(111) electrocatalyst as a function of applied potential, solution pH and related hydrogen coverage. Upon decrease of the potential, we see first a (4×4) H adlayer with 12 H adsorbates in the unit cell organized in a structure combining triangular and square patterns, followed by a restructuring of the metal catalyst itself by creation of a (4×4) array of low coordination Cu adatoms on the surface, seen for a potential of -0.32 V vs SHE at pH = 2 in the experiment. Moreover, the strong H adsorption at negative potential, associated with the high coverage, is shown to be the driving force for this restructuring. The restructured surface with Cu adatom shows lower barriers for the steps of HER than that of the Cu(111) surface, and plays a major role in the HER activity. Therefore, electroreduction conditions stabilize adatoms at the Cu surface, creating highly active sites not present on the initial catalyst. The thermodynamic equilibrium approach used here could be complemented by kinetic steady-state simulations of the formation of the restructured surface during reaction.

This work resolves the long-term controversy of the atomic structure transformation of the Cu(111) surface during the electrocatalytic process. Such restructuring originates from the low cohesive energy of Cu and strong H adsorption under reduction potential and at low pH. The results can be generalized to the restructuring of other transition metals since the chemical potential of H is determined by the electrode potential and solution pH, and the restructuring of soft coinage metals can thus be precisely controlled by these two parameters in electrocatalysis. HER is often an unwanted reaction, and, based on this work, it could be avoided by a well-chosen pH that suppresses the restructuring favorable for the HER activity. Finally, the approach can be extended to other electrochemical reactions and other adsorbates such as *CO in electrochemical CO_2 reduction reaction, and *OH or *O in electro-oxidation reactions. A similar surface roughening by formation of adatoms or small islands can be expected in these cases.

Acknowledgments

The work was supported by the National Science Foundation CBET grant 2103116. Computational resources for this work were performed on the Hoffman2 cluster at UCLA Institute for Digital Research and Education (IDRE) and the Extreme Science and Engineering Discovery Environment (XSEDE), which is supported by National Science Foundation Grant No. ACI-1548562, through allocation TGCHE170060. D.C. acknowledged George Yan from UCLA and Gong Zhang from Tianjin University for fruitful discussions.

Keywords: Global optimization • Grand canonical density functional theory • Scanning tunnelling microscopy • Surface restructuring • Hydrogen evolution reaction

[1] a) Z. W. Seh, J. Kibsgaard, C. F. Dickens, I. Chorkendorff, J. K. Norskov, T. F. Jaramillo, *Science* **2017**, *355,* 146– 157; b) Y. Y. Birdja, E. Pérez-Gallent, M. C. Figueiredo, A. J. Göttle, F. Calle-Vallejo, M. T. M. Koper, *Nat. Energy* **2019**, *4*, 732-745; c) D. F. Gao, R. M. Aran-Ais, H. S. Jeon, B. R. Cuenya, *Nat. Catal.* **2019**, *2*, 198-210; d) J. Cabana, T. Alaan, G. W. Crabtree, M. C. Hatzell, K. Manthiram, D. A. Steingart, I. Zenyuk, F. Jiao, A. Vojvodic, J. Y. Yang, N. P. Balsara, K. A. Persson, D. J. Siegel, C. L. Haynes, J. Mauzeroll, M. Shen, B. J. Venton, N. Balke, J. Rodríguez-López, D. R. Rolison, R. Shahbazian-Yassar, V. Srinivasan, S. Chaudhuri, A. Couet, J. Hattrick-Simpers, *ACS Energy Lett.* **2021**, *7*, 368-374.

[2] I. T. McCrum, M. T. M. Koper, *Nat. Energy* **2020**, *5*, 891-899.

[3] D. R. Gabe, *J. App. Electrochem.* **1997**, *27*, 908-915.

[4] B. H. R. Suryanto, C. S. M. Kang, D. Wang, C. Xiao, F. Zhou, L. M. Azofra, L. Cavallo, X. Zhang, D. R. MacFarlane, *ACS Energy Lett.* **2018**, *3*, 1219-1224.

[5] a) L. Wang, S. A. Nitopi, E. Bertheussen, M. Orazov, C. G. Morales-Guio, X. Liu, D. C. Higgins, K. Chan, J. K. Nørskov, C. Hahn, T. F. Jaramillo, *ACS Catal.* **2018**, *8*, 7445-7454; b) G. Zhang, Z. J. Zhao, D. Cheng, H. Li, J. Yu, Q. Wang, H. Gao, J. Guo, H. Wang, G. A. Ozin, T. Wang, J. Gong, *Nat. Commun.* **2021**, *12*, 5745.

[6] a) S. Nitopi, E. Bertheussen, S. B. Scott, X. Liu, A. K. Engstfeld, S. Horch, B. Seger, I. E. L. Stephens, K. Chan, C. Hahn, J. K. Norskov, T. F. Jaramillo, I. Chorkendorff, *Chem. Rev.* **2019**, *119*, 7610-7672; b) F. Dattila, R. R. Seemakurthi, Y. Zhou, N. Lopez, *Chem. Rev.* **2022**, *122*, 11085-11130.

[7] P. Grosse, D. Gao, F. Scholten, I. Sinev, H. Mistry, B. Roldan Cuenya, *Angew. Chem. Int. Ed.* **2018**, *57*, 6192-6197; *Angew. Chem.* **2018**, *130*, 6300–6305.

[8] a) P. Grosse, A. Yoon, C. Rettenmaier, A. Herzog, S. W. Chee, B. Roldan Cuenya, *Nat. Commun.* **2021**, *12*, 6736; b) D. Gao, I. Sinev, F. Scholten, R. M. Aran-Ais, N. J. Divins, K. Kvashnina, J. Timoshenko, B. Roldan Cuenya, *Angew. Chem. Int. Ed.* **2019**, *58*, 17047-17053; *Angew. Chem.* **2019**, *131*, 17203–17209. c) D. Cheng, Z. J. Zhao, G. Zhang, P. Yang, L. Li, H. Gao, S. Liu, X. Chang, S. Chen, T. Wang, G. A. Ozin, Z. Liu, J. Gong, *Nat. Commun.* **2021**, *12*, 395; d) J. Huang, N. Hormann, E. Oveisi, A. Loiudice, G. L. De Gregorio, O. Andreussi, N. Marzari, R. Buonsanti, *Nat. Commun.* **2018**, *9*, 3117; e) R. Amirbeigiarab, A. Bagger, J. Tian, J. Rossmeisl, O. M. Magnussen, *Angew. Chem. Int. Ed.* **2022**, *61*, e202211360.

[9] T. M. T. Huynh, P. Broekmann, *ChemElectroChem* **2014**, *1*, 1271-1274.

[10] B. M. Tackett, D. Raciti, A. R. Hight Walker, T. P. Moffat, *J. Phys. Chem. Lett.* **2021**, *12*, 10936-10941.

[11] Y. Xie, P. Ou, X. Wang, Z. Xu, Y. C. Li, Z. Wang, J. E. Huang, J. Wicks, C. McCallum, N. Wang, Y. Wang, T. Chen, B. T. W. Lo, D. Sinton, J. C. Yu, Y. Wang, E. H. Sargent, *Nat. Catal.* **2022**, *5*, 564-570.

[12] A. Auer, M. Andersen, E.-M. Wernig, N. G. Hörmann, N. Buller, K. Reuter, J. Kunze-Liebhäuser, *Nat. Catal.* **2020**, *3*, 797-803.

[13] a) J. Li, J. H. Stenlid, T. Ludwig, P. S. Lamoureux, F. Abild-Pedersen, *J. Am. Chem. Soc.* **2021**, *143*, 19341-19355; b) X. Liu, P. Schlexer, J. Xiao, Y. Ji, L. Wang, R. B. Sandberg, M. Tang, K. S. Brown, H. Peng, S. Ringe, C. Hahn, T. F. Jaramillo, J. K. Norskov, K. Chan, *Nat. Commun.* **2019**, *10*, 32; c) M. T. Tang, X. Liu, Y. Ji, J. K. Norskov, K. Chan, *J. Phys. Chem. C* **2020**, *124*, 28083-28092.

[14] a) G. Sun, A. N. Alexandrova, P. Sautet, *J. Chem. Phys.* **2019**, *151*, 194703; b) Z. Zhang, Z. Wei, P. Sautet, A. N. Alexandrova, *J. Am. Chem. Soc.* **2022,** *144*, 19284–19293.

[15] a) K. Mathew, V. S. C. Kolluru, S. Mula, S. N. Steinmann, R. G. Hennig, *J. Chem. Phys.* **2019**, *151*, 234101; b) S. N. Steinmann, C. Michel, R. Schwiedernoch, P. Sautet, *Phys. Chem. Chem. Phys.* **2015**, *17*, 13949-13963; c) S. N. Steinmann, P. Sautet, *J. Phys. Chem. C* **2016**, *120*, 5619-5623.

[16] D. Friebel, P. Broekmann, K. Wandelt, *Physica Status Solidi (a)* **2004**, *201*, 861-869.

[17] B. Eren, D. Zherebetskyy, L. L. Patera, C. H. Wu, H. Bluhm, C. Africh, L. W. Wang, G. A. Somorjai, M. Salmeron, *Science* **2016**, *351*, 475-478.